Appl. Phys. B 71, 259–266 (2000) / Digital Object Identifier (DOI) 10.1007/s003400000350

**Applied Physics B**
Lasers
and Optics

# Femtosecond pump–probe photoelectron spectroscopy on $Na_2$: a tool to study basic coherent control schemes

**T. Frohnmeyer**[1], **T. Baumert**[2,*]

[1] Physikalisches Institut, Universität Würzburg, 97074 Würzburg, Germany
[2] Fachbereich Physik, Universität Kassel, Heinrich Plett Str. 40, 34132 Kassel, Germany

Received: 29 October 1999/Published online: 13 July 2000 – 

**Abstract.** Femtosecond pump–probe photoelectron spectroscopy has become a common tool in ultrafast gas-phase science because of its sensitivity both to structural and electronic changes in a molecule upon excitation. Here a summary and extended discussion of our experiments is presented. We focus on the potential of this method to study basic femtosecond coherent control schemes. Multi-photon excitation of the $Na_2$ molecule with femtosecond laser pulses leads to preparation of vibrational wave packets. Mapping of the vibrational wave-packet dynamics by time-resolved photoelectron spectroscopy offers the high spatial and temporal resolution required to investigate a variety of laser-control parameters in great detail. Besides an illustration of the Tannor–Kosloff–Rice scheme we demonstrate electronic transitions at Franck–Condon forbidden internuclear distances due to the intensity of the applied laser pulses. Further we discuss the influence of simple phase-modulated (linearly chirped) laser pulses on a molecular multi-photon process. An enhanced population transfer is derived due to synchronization of the wave-packet motion on an electronic potential to an appropriate chirp of the laser pulses. In addition, the influence of the temporal profile on the population transfer and the role of the pulse duration are studied.

**PACS:** 33.60.-q; 31.70.Hq; 82.50.Fv

As the femtosecond time scale is the time scale of nuclear motion within a molecule, femtosecond laser pulses can be used either to observe or to control molecular dynamics in real-time. The corresponding research area has been termed femtochemistry [1, 2]. Different approaches for controlling chemical reactions on a femtosecond time scale are discussed for example in [3] and references therein. Most of the approaches rely on one-parameter control schemes, i.e. one laser-specific parameter is varied. In a recent experiment control was achieved by feedback-optimized phase-shaped femtosecond laser pulses [4]. In that experiment tailored femtosecond laser pulses from a computer-controlled pulse shaper [5, 6] were used to optimize the branching ratios of different organometallic photodissociation reaction channels. The optimization procedure was based on the feedback from reaction-product quantities in a learning evolutionary algorithm that iteratively improved the phase of the applied femtosecond laser pulses, leading to complex pulse shapes for the optimized laser pulses. The beauty of this method is that it works automatically and finds optimal solutions without previous knowledge of the molecular system. However, from this experiment it is non-trivial to gain insight into the individual control mechanisms that are taking place during the laser–molecule interaction and to deduce molecular information from them. In order to get a better physical insight into the multi-parameter control driving such an experiment there is a need to investigate one-parameter control schemes in detail on model systems. In that context we first have to realize that steering a molecule into a certain reaction coordinate requires multi-photon processes [7]. Further, it is advantageous to take a model system with a one-dimensional internuclear coordinate to study basic coherent control schemes, such as for example vibrations or the dissociation of a diatomic molecule. Finally, in order to detect the outcome of the control the detection method needs to be sensitive to changes in the nuclear as well as in the electronic configuration. Time-resolved multi-photon ionization on the $Na_2$ molecule [8] together with the ability to map vibrational wave-packet motion over all energetically allowed internuclear distances via photoelectron spectroscopy [9] fulfils all the above-mentioned requirements.

It should be noted that time-resolved diffraction of ultrafast electron pulses [10, 11] or X-ray pulses [12] delivers a direct method to follow structural changes in molecules upon excitation with an ultrashort laser pulse. These methods are universal in a sense that they do not need a specific detection state in comparison to commonly used pump–probe set-ups. However, they are not sensitive to changes in the electronic configuration and as they are technically rather involved they do not reach the time resolution of a few femtoseconds that we obtain nowadays by optical pump–probe methods. The latter in combination with ion-

*Corresponding author.
(Fax: +49-561/804-4453, E-mail: baumert@physik.uni-kassel.de)

or laser-induced fluorescence or ZEKE (zero kinetic energy) detection delivers high temporal resolution, but these techniques are not suited to map molecular dynamics over wide internuclear distances, as the observation of molecular dynamics relies on restricted internuclear distances for the excitation into the detection state. This limitation can be overcome, if an additional experimental parameter is found from which we are able to deduce the actual bond configuration. Experimental implementations of these ideas are for example the time-resolved up-conversion of fluorescence [13], the time-resolved detection of kinetic energy of fragments via KETOF (kinetic energy time-of-flight) techniques [14–16] or time-resolved photoelectron detection [9]. Since the first experimental demonstration of femtosecond time-resolved photoelectron spectroscopy [17] this technique has developed rapidly into a common tool in ultrafast gas-phase science because of its sensitivity both to structural and electronic changes in a molecule upon excitation [18–25]. Recent developments are extending the technique by the use of imaging devices in order to facilitate the detection of the electrons' angular distribution [23, 26] and by coincidence techniques [22, 26]. Theoretically the method was described by Seel and Domcke [27] first and applied by Meier and Engel [28] to the mapping of vibrational wave-packet motion that we have demonstrated experimentally [9]. Current research topics are the calculation of the angular distribution of the photoelectrons and the evolution of electronic structure with femtosecond time resolution [29].

In this contribution we will focus on femtosecond pump–probe photoelectron spectroscopy as a tool to study basic coherent control schemes. After a short introduction into the experimental set-up and the relevant multi-photon ionization dynamics of the $Na_2$ molecule we will first give an extended discussion of our mapping experiment [9], before we discuss the individual control schemes investigated by this technique.

## 1 Experimental set-up

The femtosecond laser pulses are provided by a home-built Ti:sapphire oscillator with a chirped pulse amplification (CPA) system. The pulses of 800 nm (90 fs, 1 mJ, 1 kHz) are frequency-converted into pulses of 620 nm having a maximum energy of 20 μJ and a minimum pulse duration of 40 fs by employing an optical parametric generator (OPG) including a subsequent prism compressor. In a Michelson-type set-up the beam is split into two equal parts and a variable time delay is introduced. Both beams can be attenuated separately to adjust the intensity of the pump and probe lasers. The recombined laser beams are focused with a 300 mm lens into the vacuum chamber where the laser interacts with the molecular beam. The sodium dimer is prepared vibrationally cold by supersonic expansion of sodium from an oven operated at 900 K through a nozzle of 200-μm-diameter orifice into a differentially pumped vacuum chamber. The beam is skimmed and directed through the pole-pieces of a magnetic-bottle electron spectrometer [30] (MBES, Applied Laser Technology) where it intersects the laser beam perpendicular; in an earlier phase of the experiments a $\mu$-metal-shielded linear time-of-flight (TOF) spectrometer was used. The photoelectron spectra are recorded by their TOF distribution in the MBES using a 1 GHz, 2 giga-sample digital oscilloscope and averaged over several thousands of laser shots.

Calibration was performed using $2+1$ REMPI (resonance-enhanced multi-photon ionization) with the help of a tunable nanosecond dye laser via the Na $4d$ and $3d$ levels, yielding known photoelectron energies of 1.286 eV and 0.286 eV respectively. The energy resolution was determined to be 30 meV for electrons with a kinetic energy of 0.7 to 1.0 eV. By applying a retardation field we obtain an energy resolution of 20 meV at 0.5 eV. Because of the high efficiency in electron collection of a MBES it is possible to perform the measurements at low densities of $Na_2$ in the interaction region. This is crucial in order to minimize space-charge effects in strong laser fields. In addition a linear TOF mass spectrometer is used to detect the corresponding ions. This enables us to compare the excitation conditions in the photoelectron experiment to the well-studied multi-photon ionization dynamics of $Na_2$ (at 2 eV photon-energy excitation) [8, 31].

## 2 Excitation scheme and difference-potential analysis

The excitation scheme of the experiment is depicted in Fig. 1. At 620 nm three photons are needed to ionize the $Na_2$ molecule from its neutral ground state $X\,^1\Sigma_g^+$ into its ionic ground state $^2\Sigma_g^+$. The dynamical aspect of this multi-photon excitation has been investigated in this wavelength regime in detail with ion detection [8]. Due to the spectral width of the laser pulse and due to the Franck–Condon principle one-photon excitation prepares a wave packet at the inner turning point of the $A\,^1\Sigma_u^+$-state potential by coher-

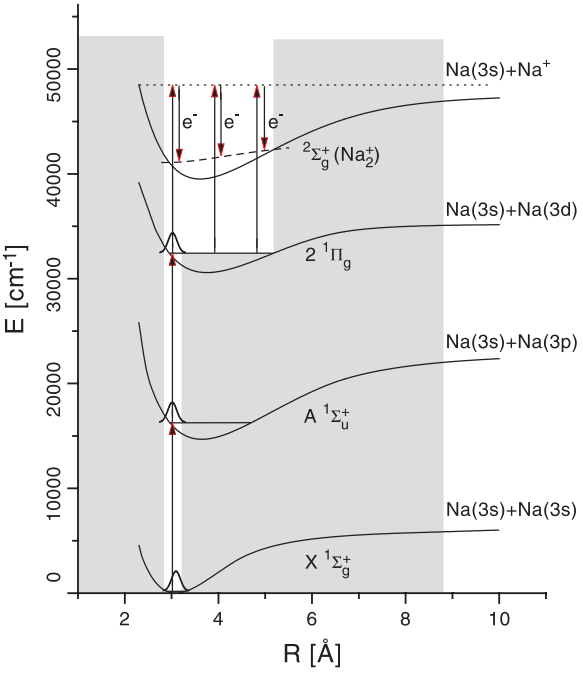


**Fig. 1.** Excitation scheme. The pump laser at 620 nm creates wave packets in the $A\,^1\Sigma_u^+$ and the $2\,^1\Pi_g$ at the inner turning points. The time-delayed probe laser ionizes the sodium dimer. As indicated the kinetic energy of the photoelectrons depends on the internuclear coordinate because of the monotonically increasing difference potential (*dashed line*, see text)

ent superposition of vibrational levels. The roundtrip time of this wave packet is about 310 fs ( $\approx 110\,\mathrm{cm}^{-1}$). Two-photon excitation leads to preparation of a wave packet at the inner turning point of the $2\,^1\Pi_g$-state potential with a roundtrip time of about 370 fs ($\approx 90\,\mathrm{cm}^{-1}$). In [8] it was found that the $A\,^1\Sigma_u{}^+$-state wave-packet motion is reflected in the total $Na_2^+$-ion yield due to a resonance-enhanced 'direct' photoionization process via the $2\,^1\Pi_g$ state into the $Na_2^+$ ($^2\Sigma_g{}^+$) state at the inner turning point of the molecular potential curves involved (see Fig. 1). In those experiments the $2\,^1\Pi_g$-state wave-packet motion could only be detected in the $Na_2^+$ and $Na^+$ fragment signal due to the excitation of a doubly excited neutral state of the $Na_2$ molecule near the outer turning point of the $2\,^1\Pi_g$-state potential (not shown in Fig. 1) and its subsequent decay channels as autoionization (indirect photoionization) and autoionization-induced fragmentation [8, 32]. Note that 'direct' photoionization out of the $2\,^1\Pi_g$-state into the $Na_2^+$ ($^2\Sigma_g{}^+$) state cannot provide the dynamical information on the wave-packet prepared on this state when detected by the total $Na_2^+$-ion yield, since a large part of internuclear distances is sampled in a pump–probe experiment [33, 34]. However, by the detection of kinetic-energy-resolved photoelectrons this dynamical information can be obtained, because electrons of different kinetic energies are formed at different internuclear distances. In such a direct photoionization process the released kinetic energy of the photoelectrons can be determined by a classical difference-potential analysis [33, 35]: let $E_1$ and $E_2$ denote the total energy of the nuclei in molecular potentials $V_1(R)$ and $V_2(R)$ before and after the absorption of a photon with energy $h\nu$. Due to the Franck–Condon principle the nuclei will not noticeably change either their relative position or their velocities during an electronic transition. This means the transition occurs at a fixed internuclear distance and will conserve the kinetic energy $E_{\mathrm{kin}}(R)$. For a transition between neutral states the energy net result can be written as: $V_1(R) + E_{\mathrm{kin}}(R) + h\nu = V_2(R) + E_{\mathrm{kin}}(R) \Leftrightarrow V_2(R) - V_1(R) = h\nu$. Graphically the classical transition is given by the intersection of a horizontal line with height $h\nu$ with the difference potential $V_2(R) - V_1(R)$. Considering transitions between a neutral and an ionic state we have to modify this analysis slightly, as the ejected electron carries away the excess kinetic energy $E_{\mathrm{electron}}$ and we obtain $V_2(R) - V_1(R) = h\nu - E_{\mathrm{electron}} \leq h\nu$. Often it is convenient to shift the difference potential with respect to $E_1$, so that we can analyse the excitation within the potential-energy diagram. The dashed line in Fig. 1 displays the difference potential $^2\Sigma_g{}^+$ ($Na_2^+$) $- 2\,^1\Pi_g + 2\,\mathrm{h}\nu$ relevant for this experiment. Accordingly, the expected photoelectron energy in this photoionization process out of the $2\,^1\Pi_g$ state is decreasing with increasing internuclear distance. At the inner turning point of the potential curve photoelectrons of about 0.94 eV are formed whereas at the outer turning point photoelectrons of about 0.78 eV are released. Recording transient photoelectron spectra enables us to probe molecular wave-packet motion on neutral electronic states along all energetically allowed internuclear distances simultaneously. Note that the autoionization processes of the doubly excited state lead to photoelectrons with less than 0.5 eV kinetic energy [32], which can be well separated from the electrons released in the 'direct' photoionization process.

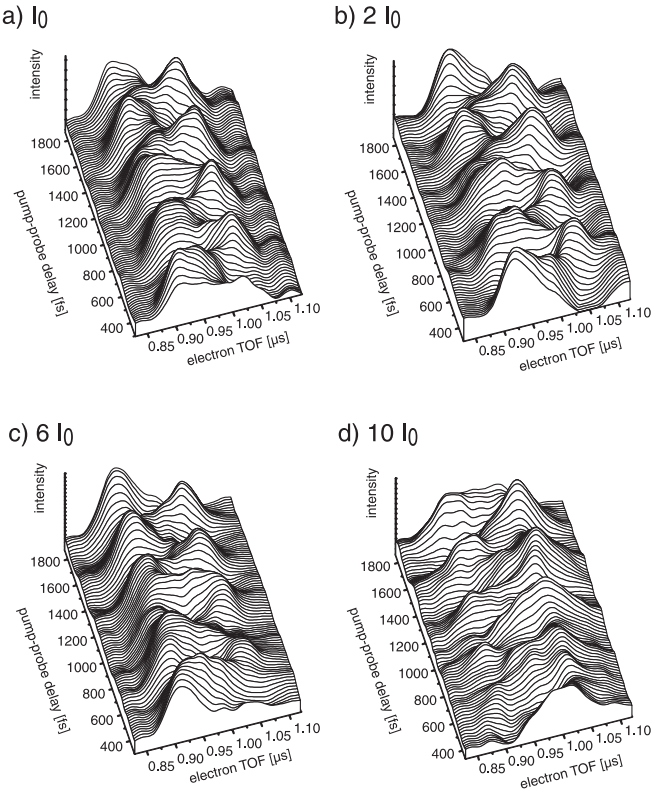


**Fig. 2a–d.** TOF (time-of-flight) photoelectron distributions for a fixed pump-laser intensity ($I_0 \approx 10^{11}\,\mathrm{W/cm^2}$) and increasing probe-laser intensity; **a** $I_{\mathrm{probe}} = I_0$, **b** $I_{\mathrm{probe}} = 2I_0$, **c** $I_{\mathrm{probe}} = 6I_0$, **d** $I_{\mathrm{probe}} = 10I_0$. The wave-packet dynamics on the neutral electronic states is mapped

## 3 Mapping and inversion

In Fig. 2a the measured TOF photoelectron distribution is shown as a function of the pump–probe delay for the same in-

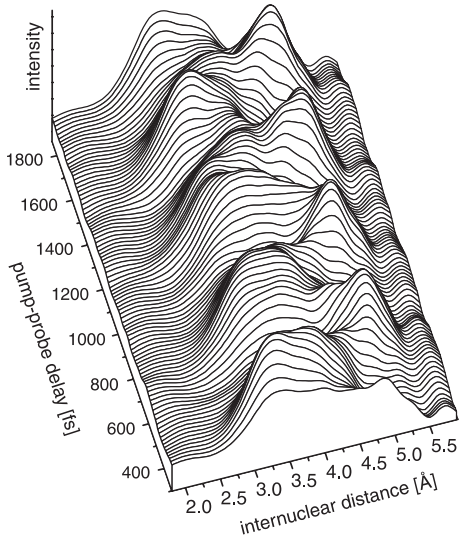


**Fig. 3.** After calibration of the TOF electron spectrometer with the help of atomic resonances, the TOF axis from Fig. 2a is converted into an energy axis. Taking the difference potential into account the mapped wave-packet dynamics as a function of the internuclear distance is obtained with sub-Å spatial resolution

tensity ($I_0 \approx 10^{11}$ W/cm$^2$; 70 fs; 620 nm) of pump and probe lasers. The TOF range from 0.8 μs to 1.15 μs displayed in the figure corresponds to a kinetic energy of the electrons from 1.1 eV to 0.6 eV. Variation of the pump–probe delay monitors the dynamics of the molecule in the two neutral states $2\,^1\Pi_g$ and $A\,^1\Sigma_u{}^+$ (via the $2\,^1\Pi_g$). Particularly the propagation of the $2\,^1\Pi_g$ wave packet between the turning points is resolved. In order to obtain the mapped wave-packet dynamics as a function of the internuclear distance R we transformed the TOF axes to the corresponding kinetic-energy axis and took the difference potential $^2\Sigma_g{}^+(\mathrm{Na}_2^+) - 2\,^1\Pi_g + 2h\nu$ into account. The result is displayed in Fig. 3. Taking the slope of the difference potential, the energy resolution of our spectrometer and the energetic width of our fs laser pulses into account we obtain a spatial resolution of about 0.5 Å.

In order to deduce more dynamical information we performed a fast Fourier transformation (FFT) of the photoelectron distribution along the pump–probe delay. Cuts of this two-dimensional FFT at 0.9 μs and 1.02 μs time-of-flight, corresponding to the inner and the outer turning point of the wave packets in the $2\,^1\Pi_g$ state, are displayed at the top of Fig. 4. There are two dominant contributions to the whole dynamics in the Fourier spectrum at about 90 cm$^{-1}$ and 110 cm$^{-1}$ originating from the wave packets in the $2\,^1\Pi_g$ and the $A\,^1\Sigma_u{}^+$ states, respectively. At the inner turning point we observe both contributions whereas at the outer turning point there is just the signal at 90 cm$^{-1}$. This can be explained in terms of the difference-potential picture of the $A\,^1\Sigma_u{}^+$ and $2\,^1\Pi_g$ states depicted in Fig. 5 and also discussed in [8, 33]. With attenuated laser intensities a resonance-enhanced ionization out of the $A\,^1\Sigma_u{}^+$ state via the $2\,^1\Pi_g$ state is allowed at internuclear distances, where the difference potential equals the photon energy. Therefore in the sodium dimer there is a Franck–Condon window in the transition probability limited to the region of the inner turning point of the wave-packet propagation in the $A\,^1\Sigma_u{}^+$ state, which is indicated in Fig. 1 for clarity. As a consequence we observe a resonance-enhanced transition at the inner turning point of the wave packet in the $A\,^1\Sigma_u{}^+$ state but none at its outer turning point. The wave-packet propagation in the $2\,^1\Pi_g$ state can be observed at all allowed internuclear distances since in this direct ionization process there is no limitation to a specific internuclear distance.

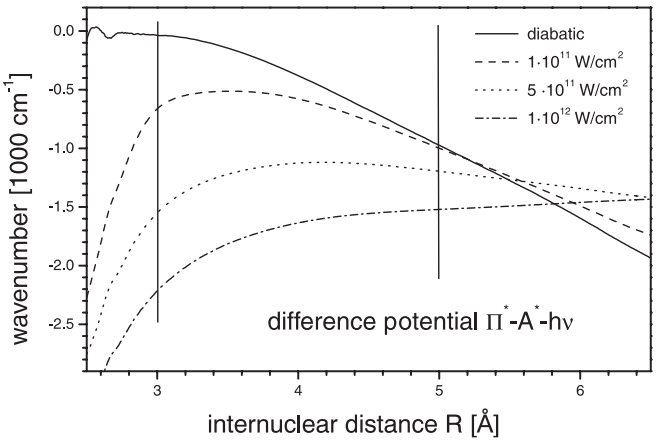


**Fig. 5.** Difference potential calculated in an adiabatic picture for different laser intensities. In the diabatic limit the difference potential $\Pi^*$-$A^*$-$h\nu$ equals the photon energy at small internuclear distances $R$ and decreases with increasing $R$ (*solid line*). At an intensity of $5 \times 10^{11}$ W/cm$^2$ the potential is almost flat in the relevant region of $R$

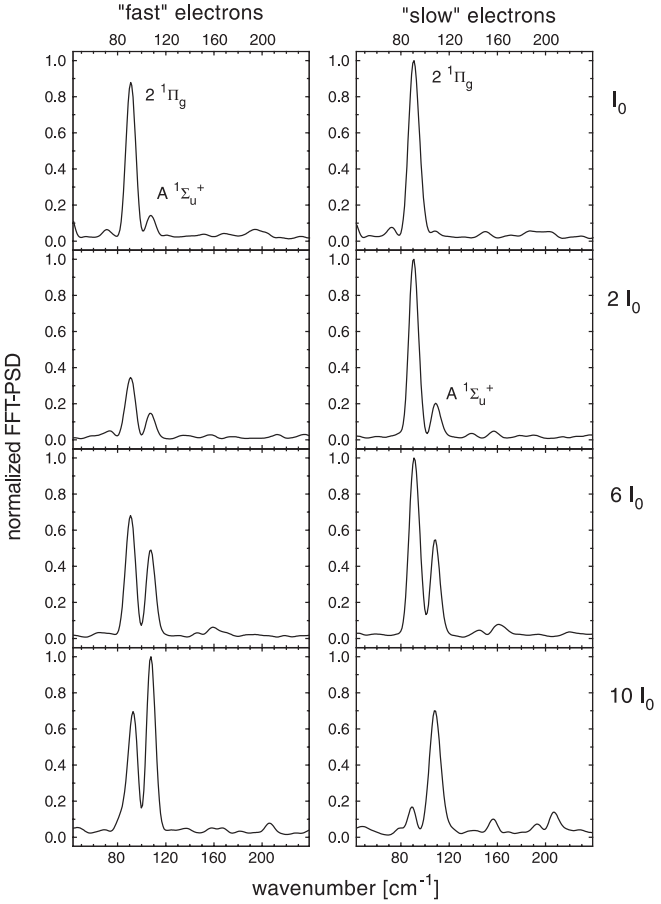


**Fig. 4.** Cuts of the normalized FFT spectra obtained from Fig. 2 at two fixed TOFs, representing the inner (*left*, 0.90 μs) and the outer (*right*, 1.02 μs) turning points of the wave packets. By increasing the probe-laser intensity the contribution of the $A\,^1\Sigma_u{}^+$ wave packet for the 'fast' photoelectrons increases in relation to the $2\,^1\Pi_g$ wave packet. For 'slow' photoelectrons the contribution of the $A\,^1\Sigma_u{}^+$ wave packet starts to appear at intermediate intensities and increases rapidly with increasing laser intensity. This behaviour is attributed to the effect of perturbed molecular potentials in high laser fields (dressed states). The minor-frequency contributions are attributed to ground-state contribution and harmonics of the $A\,^1\Sigma_u{}^+$ and $2\,^1\Pi_g$ wave packets

## 4 Basic one-parameter control schemes

### *4.1 The Tannor–Kosloff–Rice scheme*

In the time domain the so-called Tannor–Kosloff–Rice scheme [36] is a very illustrative way of how to obtain control over different products via photoexcitation of a molecule. They have proposed that controlling the time duration of a wave packet on an excited electronic potential-energy surface can be used to achieve different products. In practice this means that a pump laser prepares a vibrational wave packet on an electronic excited potential and with the help of a time-delayed probe laser the product state is populated either by dumping the wave packet down again or by further excitation. In our case studied here we obtain a higher kinetic energy

of photoelectrons at the inner turning point and a lower kinetic energy of the photoelectrons at the outer turning point from the ionization of a vibrational wave packet propagating on the $2\,^1\Pi_g$ state (see Fig. 1). If we consider the electrons with different energy as different photoproducts it is evident from Fig. 2a that by controlling the duration of the wave packet on the $2\,^1\Pi_g$ state we have access to different product states. Note that at the outer turning point we have access to a doubly excited neutral state that decays inter alia via fragmentation [8, 32]. By this means we demonstrated the control of the photoproduct ratio $Na^+/Na_2^+$ in a pump–probe experiment [8, 37]. Further experimental examples employing this scheme can be found for example in [38] on the NaI molecule and in [39] on the XeI system. In general, the wavelength range needed for the excitation of the wave packet will differ from the wavelength range needed to reach the product state at a certain bond configuration due to Franck–Condon arguments. If the Tannor–Kosloff–Rice scheme were the only way to reach a desired product, then feedback-optimized phase-shaped femtosecond laser pulses might not find the optimal solution in cases where the two wavelength regimes are not contained in the spectral width of the laser pulse. A possible solution can be found by investigating effects that depend on the intensity of the probe laser as discussed in Sect. 4.2.

### *4.2 Intensity of the laser pulses*

First we have to distinguish between effects due to intensity variations of the pump pulse and those due to the probe pulse. In earlier experiments we have demonstrated that an increased intensity for the pump process in our excitation scheme (Fig. 1) leads to Rabi-type cycles (molecular '$\pi$ pulses') of the population in the relevant electronic states [31, 40]. Now we will focus on recent experiments [41] where we have varied the intensity of the probe laser. We have found that the increase of the probe-laser intensity gives rise to electronic transitions at internuclear distances that are not allowed in the perturbation regime due to Franck–Condon arguments.

In a set of measurements the pump-laser intensity is kept fixed whereas the probe-laser intensity is increased from $I_0 \approx 10^{11}\,\mathrm{W/cm^2}$ to $10I_0$. As the excitation of the wave packets is identical in the whole set of experiments the population and the time evolution in the intermediate states are also identical. The propagation of the vibrational wave packets over all allowed internuclear distances is monitored with a probe laser of variable intensity to detect the influence of high laser intensities on the molecular potential sensitive to the internuclear distance. The photoelectron signals for probe-laser intensities ranging from $I_0$ to $10I_0$ are shown in Fig. 2. The dynamical behaviour changes as a function of the intensity, and the kinetic energy of the time-of-flight of the photoelectrons is slightly increased corresponding to a decrease of the photoelectron energy ($\approx 0.03\,\mathrm{eV}$). In Fig. 4 the FFT of the cuts at TOFs corresponding to the inner and outer turning points of the wave packets are shown. As mentioned before, at the inner turning point we observe signals of the wave packet in both the $A\,^1\Sigma_u{}^+$ and the $2\,^1\Pi_g$ state. With increasing probe-laser intensity the ratio of the signals in the FFT changes and the signal of the wave packet in the $A\,^1\Sigma_u{}^+$ state becomes dominant compared to that in the $2\,^1\Pi_g$ state. As mentioned above, there is no contribution of the $A\,^1\Sigma_u{}^+$-state wave packet at the attenuated probe-laser intensity at the outer turning point. At an intermediate probe intensity of $2I_0$ we observe the onset of the frequency corresponding to the $A\,^1\Sigma_u{}^+$ wave packet. This contribution increases rapidly with increasing probe-laser intensity and is dominant for the highest intensity used ($10I_0$). At $6I_0$ the signal heights of the wave-packet contributions in the FFT at the inner and the outer turning point become comparable. The increasing contribution of the frequency of the $A\,^1\Sigma_u{}^+$ wave packet with increasing probe-laser intensity as compared to the frequency of the $2\,^1\Pi_g$ wave packet at the inner turning point might be attributed to the increased probability of two-photon absorption processes at high laser intensities. The electronic transition at the outer turning point out of the $A\,^1\Sigma_u{}^+$ state with increasing probe-laser intensities, however, cannot be explained by nonresonant two-photon ionization, because this process implies a constant photoelectron energy for all allowed internuclear distances, since the difference potential between the $A\,^1\Sigma_u{}^+$ state and the ionic ground state is flat. An explanation of this behaviour is possible in terms of light-induced potentials (see for example [42] and references therein). Within this concept the laser intensity affects the molecular potentials leading to adiabatic potentials. First theoretical calculations were performed using the split-operator technique [43] [44] and involving the $X\,^1\Sigma_g{}^+$, $A\,^1\Sigma_u{}^+$ and $2\,^1\Pi_g$ states. The transition-matrix elements are supposed to be independent of the internuclear distance. The coupling to the ionic ground state is treated by perturbation theory, since the transition-matrix elements are about ten times smaller than those in the neutral system [45]. Since the concept of difference potentials is capable of explaining the photoelectron signal at attenuated laser intensities, i.e. where perturbation theory holds, we transferred this concept to higher intensities. For that purpose we considered the calculated adiabatic dressed states for each laser intensity, denoted in the following as $A^*$ and $\Pi^*$. At the limit of attenuated laser intensities this adiabatic difference potential passes into the diabatic potential (Fig. 5) and the statements derived within the perturbation theory hold as discussed above. At a laser intensity of about $5 \times 10^{11}\,\mathrm{W/cm^2}$ the adiabatic difference potential becomes almost flat over internuclear distances where the molecular wave-packet motion takes place (i.e. 3–5 Å). Within this context there is no restriction for the transition between the $A^*$ and the $\Pi^*$ states to a specific molecular configuration as in the diabatic limit and thus the transition probability is independent of the internuclear distance. At a laser intensity of $10I_0$ the adiabatic difference potential even increases with increasing internuclear distance, resulting in a restriction of internuclear distances where transitions from $A^*$ to $\Pi^*$ can take place. As explained these adiabatic difference potentials give evidence to a change in the relative transition probability between the neutral adiabatic $A^*$ and $\Pi^*$ states in the sodium dimer. As a function of the probe-laser intensity the dependence on the internuclear distance of this probability changes. The kinetic energy of the photoelectrons is determined by the difference potential between the $\Pi^*$ state and the ionic ground state. According to the calculations the monotonically increasing slope of this difference potential is similar for all laser intensities used. Therefore the relation between the kinetic energy and the internuclear distance is given at high laser intensities as in the limit of low intensity (see Fig. 1). As a consequence

the different contribution of the dynamics in the $A\,^1\Sigma_u{}^+$ state to the whole dynamics for increasing laser intensity is determined by the change of the difference potential between the adiabatic $A^*$ and the $\Pi^*$ state. Within this concept the frequency of the A wave packet at a laser intensity of $6I_0$ can be observed in the photoelectron spectrum independent of the internuclear coordinate, since there is no limitation to a Franck–Condon window for a resonant ionization out of the $A^*$ state via the $\Pi^*$ state. Calculating the photoelectron energy in our approach we expect a decrease with increasing probe-laser intensity of about 0.2 eV. This is more than the observed energetic shift of about 0.03 eV corresponding to the measured TOF of the photoelectrons. This might be an effect of a light-induced coupling of electronic states in the ionic system leading to a shift in the ionic ground-state potential [42], which was not included in our calculations. The Gaussian variation of the laser intensity across the spatial beam profile was also not taken into account. Full theoretical calculations to study the observed behaviour are currently being performed [46]. At the highest probe-laser intensities used in this experiment the further absorption of photons in the continuum is observed. The discussion of molecular above-threshold ionization (ATI) on the $Na_2$ system was the subject of a recent publication [47].

### *4.3 Chirp and pulse duration of the laser pulses*

In the last couple of years an increasing number of experiments has been devoted to the use of phase-shaped laser pulses in order to control atomic and molecular properties. Linearly chirped laser pulses were used to control the population in atomic two- and three-level systems [48, 49] as well as in the B–X system of the $I_2$ molecule [50]. In those experiments control over population was achieved by making use of adiabatic rapid passage in intense linearly chirped laser pulses, whereas in a recent theoretical publication such a scheme is proposed as a method to produce molecular $\pi$ pulses with inversion probabilities of up to 99% [51]. A shaped vibrational wave packet was obtained via excitation with linearly chirped pulses in the $B$ state of $I_2$ [52] and the $E$ state of $Li_2$ [53]. Control of the population in the ground and excited states of the laser dye LD 690 was also reported by this means [54]. In order to shape atomic Rydberg wave packets a computer-controlled pulse shaper was employed [55, 56] and by a similar method a phase shift between two fs pulses was used in an experiment on Na atoms [56]. Recently an increase in the $Na^*$ yield from photodissociation of NaI [57] was observed as well as of the $I_2{}^*$ yield from photodissociation of $CH_2I_2$ and from excitation of $I_2$ [58, 59] employing simple phase-shaped laser pulses.

In the following we will report on the observation of a strong chirp dependence of the three-photon ionization probability of $Na_2$ using simple phase-shaped femtosecond laser pulses. For a detailed discussion of that experiment see [60].

Figure 6a shows photoelectron spectra obtained from ionizing $Na_2$ with up-chirped, unchirped and down-chirped laser pulses at 620 nm. The chirped pulses were produced by increasing or decreasing the optical pathway in a prism sequence (SF10) that is used to compress the pulses coming out of the OPG to their transform limit of 40 fs. The

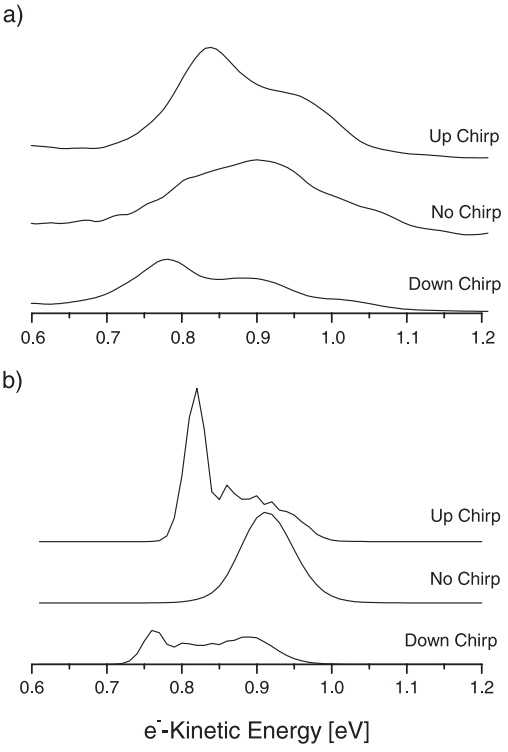


**Fig. 6. a** Electron spectra measured with single up-chirped ($+3500\,\mathrm{fs}^2$), down-chirped ($-3500\,\mathrm{fs}^2$) and unchirped laser pulses. The transform-limited pulses of 40 fs duration are centred at a wavelength of 618 nm. The chirped pulses are of 240 fs duration. **b** Calculated spectra using the same parameters as above

upper and lower spectra in Fig. 6a were obtained with linearly chirped pulses ($3500\,\mathrm{fs}^2 \pm 500\,\mathrm{fs}^2$) which corresponds to a pulse duration of approximately 240 fs. The ionization yield is seen to double when the frequency order is switched from blue first to red first in the exciting laser pulse. Note that the up- and down-chirped pulses are identical in all their pulse parameters, except for being reversed in time. This indicates that the change in the electron spectra is indeed due to the phase modulation and not to other effects such as different pulse durations or different intensity distributions. In order to better understand the experimental results, we performed quantum-mechanical calculations following the method employed in [61, 62]. In these calculations we included the electric field of a linearly chirped Gaussian laser pulse in analytical form (see e.g. [63]). In accordance with the experimental conditions (the laser beam was attenuated appropriately) calculations were performed in the weak-field limit taking into account the $X\,^1\Sigma_g{}^+$, $A\,^1\Sigma_u{}^+$ and $2\,^1\Pi_g$ neutral electronic states and coupling the $2\,^1\Pi_g$ state to the discretized continuum of the ionic ground state $^2\Sigma_g{}^+$ ($Na_2^+$). R-independent dipole-matrix elements were assumed for all transitions. The calculated electron spectra depicted in Fig. 6b qualitatively reproduce the measured results. In addition, the population in the $2\,^1\Pi_g$ state as a function of time was calculated for both chirp directions, which is shown in Fig. 7.

Since the Franck–Condon maximum for both the $A\,^1\Sigma_u{}^+ \leftarrow X\,^1\Sigma_g{}^+$ state transition as well as for the $2\,^1\Pi_g \leftarrow A\,^1\Sigma_u{}^+$ state transition is shifted towards the red of the central laser wavelength, the up-chirped laser pulse transfers population to

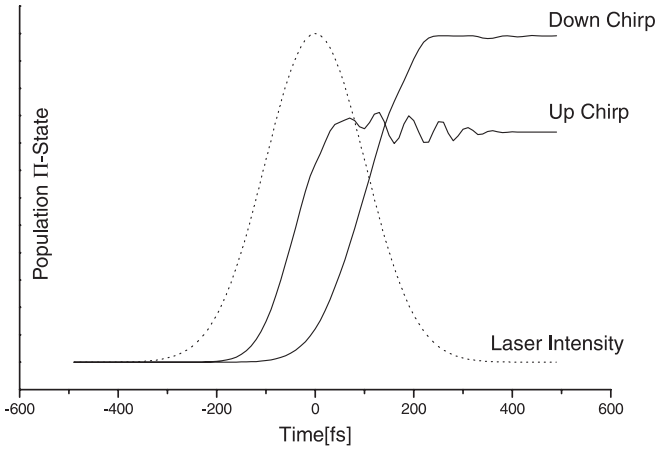


**Fig. 7.** Calculated temporal development of the population in the $2\,^1\Pi_g$ state during interaction with up- and down-chirped laser pulses ($\pm 3500\,\mathrm{fs}^2$). The chirped-pulse profile is shown as a *dotted line*

the excited states earlier, while a down-chirped laser pulse can efficiently excite the intermediate states only with its trailing edge. For the subsequent ionization process this temporal behaviour is essential. In order to achieve a high ionization yield the population in the $2\,^1\Pi_g$ state must be high at the maximum laser intensity, which is achieved with up-chirped but not with down-chirped laser pulses.

However, Fig. 7 also yields a very surprising result. The total population transferred to the $2\,^1\Pi_g$ state after the end of the pulse is much larger for a down-chirped laser although the ionization yield with this pulse is smaller. This is not due to population transfer to the ionic ground state since in the weak-field limit ionization does not (significantly) decrease the neutral-state population. Rather a mechanism very similar to that observed in the experiments described in [54] is responsible for this effect. A semiclassical argument based on the difference-potential analysis is very illuminating for the interpretation of this effect. When a chirped laser pulse is used the photon energy $h\nu$ is changing in time. For a down-chirped pulse the decreasing laser frequency follows the decrease in the difference potential $2\,^1\Pi_g - A\,^1\Sigma_u{}^+$ as the excited $A\,^1\Sigma_u{}^+$-state wave packet propagates to larger internuclear distances (see Fig. 5 in the diabatic limit). Excitation is classically allowed over a wider range of the nuclear coordinate for a down-chirped laser pulse and thus the corresponding final population in the $2\,^1\Pi_g$ state is higher. With the opposite chirp direction (up-chirp) on the other hand one observes a higher ionization yield while the intermediate-state population is kept low. This kind of optimization is desired in coherent control schemes. Besides the strong chirp dependence of the ionization yield observable in the electron spectra shown Fig. 6, a very different electron signal is observed for unchirped 40 fs laser pulses compared to the chirped laser pulses of 240 fs duration ($3500\,\mathrm{fs}^2$). The short laser pulse predominantly yields electrons with kinetic energy of about 0.9 eV; the electron spectra obtained with the longer (chirped) pulses are dominated by electrons around 0.8 eV. This behaviour can again be understood in the picture of the difference-potential analysis, this time for the transition from the $2\,^1\Pi_g$ state to the ionic ground state (see Fig. 1). Since this difference potential is increasing with internuclear distance, the electrons released have less kinetic energy when formed at the outer turning point of a wave packet propagating in the $2\,^1\Pi_g$ potential, compared to those formed at the inner turning point (see Fig. 1). The duration of the transform-limited 40 fs pulse is much shorter than the oscillation period (approx. 370 fs) of the excited vibrational levels of the $2\,^1\Pi_g$ state, and therefore the wave packet has no time to move to large internuclear distances during the laser interaction. The up- and down-chirped laser pulses, however, are of much longer duration, which allows the wave packets to sweep the whole range of allowed internuclear distances while ionization takes place. The resulting electron spectra therefore extend to lower kinetic energies, which correspond to the outer turning point where the wave packets spend more time. Using pulses of different duration it is also possible to influence the fragmentation of $Na_2$ as discussed in [60].

## 5 Conclusion

In this contribution we have demonstrated the potential of femtosecond pump–probe photoelectron spectroscopy applied to the multi-photon ionization of the $Na_2$ molecule for the study of basic coherent control schemes. Mapping of vibrational wave-packet motion with high spatial and temporal resolution is a key feature of this approach, which allowed us to study a variety of one-parameter control schemes in great detail. Based on this knowledge a comparison to results of feedback-optimized laser pulses applied to this system will give insight into the composition of an automated multi-parameter control scheme. Going to larger molecules, control schemes on isomerization and energy-redistribution processes can be studied using this method because of its sensitivity both to structural and electronic changes in a molecule upon excitation.

*Acknowledgements.* The authors have performed the experiments presented in this contribution together with A. Assion, M. Geisler, J. Helbing, M. Hofmann, V. Seyfried, M. Strehle and D. Wössner in the laboratories of G. Gerber at the University of Würzburg. Fruitful discussions with G. Gerber and V. Engel are acknowledged. Financial support was given by the Deutsche Forschungsgemeinschaft through the Schwerpunktsprogramm: 'Femtosekunden-Spektroskopie elementarer Anregungen in Atomen, Molekülen und Clustern'.

## References

1. A.H. Zewail: Femtochemistry – Ultrafast Dynamics of the Chemical Bond I & II (World Scientific, New Jersey, Singapore 1994)
2. J. Manz, L. Wöste (Eds.): Femtosecond Chemistry (VCH, Weinheim 1995)
3. P. Gaspard, I. Burghardt (Eds.): Chemical Reactions and Their Control on the Femtosecond Time Scale – XXth Solvay Conference on Chemistry (New York, John Wiley 1997)
4. A. Assion, T. Baumert, M. Bergt, T. Brixner, B. Kiefer, V. Seyfried, M. Strehle, G. Gerber: Science **282**, 919 (1998)
5. A.M. Weiner, D.E. Leaird, J.S. Patel, J.R. Wullert: IEEE J. Quantum Electron. **QE-28**, 908 (1992)
6. T. Baumert, T. Brixner, V. Seyfried, M. Strehle, G. Gerber: Appl. Phys. B **65**, 779 (1997)
7. P. Brumer, M. Shapiro: Chem. Phys. **139**, 221 (1989)
8. T. Baumert, M. Grosser, R. Thalweiser, G. Gerber: Phys. Rev. Lett. **67**, 3753 (1991)
9. A. Assion, M. Geisler, J. Helbing, V. Seyfried, T. Baumert: Phys. Rev. A **54**, R4605 (1996)

10. J.C. Williamson, M. Dantus, S.B. Kim, A.H. Zewail: Chem. Phys. Lett. **196**, 529 (1992)
11. J. Cao, H. Ihee, A.H. Zewail: Chem. Phys. Lett. **290**, 1 (1998)
12. F. Ráksi, K.R. Wilson, Z. Jiang, A. Ikhlef, C. Y. Côté, J.-C. Kieffer: J. Chem. Phys. **104**, 6066 (1996)
13. T.J. Dunn, I.A. Walmsley, S. Mukamel: Phys. Rev. Lett. **74**, 884 (1995)
14. T. Baumert, S. Pedersen, A.H. Zewail: J. Phys. Chem. **97**, 12 447 (1993)
15. A. Assion, T. Baumert, M. Geisler, V. Seyfried, G. Gerber: Euro. Phys. J. D **4**, 145 (1998)
16. H. Stapelfeldt, E. Constant, P.B. Corkum: Phys. Rev. Lett. **74**, 3780 (1995)
17. D.R. Cyr, C.C. Hayden: J. Chem. Phys. **104**, 771 (1995)
18. B.J. Greenblatt, M.T. Zanni, D.M. Neumark: Chem. Phys. Lett. **258**, 523 (1996)
19. P. Ludowise, M. Blackwell, Y. Chen: Chem. Phys. Lett. **258**, 530 (1996)
20. C. Jouvet, S. Martrenchard, D. Solgadi, C. Dedonder-Lardeux, M. Mons, G. Grégoire, I. Dimicoli, F. Piuzzi, J.P. Visticot, J.M. Mestdagh, P. D'Oliveira, P. Meynadier, M. Perdrix: J. Phys. Chem. A **101**, 2555 (1997)
21. V. Stert, W. Radloff, T. Freudenberg, F. Noack, C. Jouvet, Femtochemistry-III. Lund, Sweden: Book of abstracts, Reprocentralen Kemicentrum Lund 1997
22. V. Stert, W. Radloff, C.P. Schulz, I.V. Hertel: Euro. Phys. J. D **5**, 97 (1999)
23. L. Wang, H. Kohguchi, T. Suzuki: Faraday Discuss. **113**, 27 (1999)
24. G. Ganteför, S. Kraus, W. Eberhardt: J. Electr. Spectr. Rel. Phen. **35**, 88 (1997)
25. V. Blanchet, M. Zgierski, T. Seideman, A. Stolow: Nature **401**, 52 (1999)
26. J.A. Davies, J.E. LeClaire, R.E. Continetti, C.C. Hayden: J. Chem. Phys. **111**, 1 (1999)
27. M. Seel, W. Domcke: J. Chem. Phys. **95**, 7806 (1991)
28. C. Meier, V. Engel: Chem. Phys. Lett. **212**, 691 (1993)
29. Y. Arasaki, K. Takatsuka, K. Wang, V. McKoy: Chem. Phys. Lett. **302**, 363 (1999)
30. P. Kruit, F.H. Read: J. Phys. E: Sci. Instrum. **16**, 313 (1983)
31. T. Baumert, V. Engel, C. Meier, G. Gerber: Chem. Phys. Lett. **200**, 488 (1992)
32. T. Baumert, B. Buehler, R. Thalweiser, G. Gerber: Phys. Rev. Lett. **64**, 733 (1990)
33. T. Baumert, B. Buehler, M. Grosser, R. Thalweiser, V. Weiss, E. Wiedenmann, G. Gerber: J. Phys. Chem. **95**, 8103 (1991)
34. V. Engel: Chem. Phys. Lett. **178**, 130 (1991)
35. R.S. Mulliken: J. Chem. Phys. **55**, 309 (1971)
36. D.J. Tannor, R. Kosloff, S.A. Rice: J. Chem. Phys. **85**, 5805 (1986)
37. T. Baumert, G. Gerber: Adv. At. Molec. Opt. Phys. **35**, 163 (1995)
38. J.L. Herek, A. Materny, A.H. Zewail: Chem. Phys. Lett. **228**, 15 (1994)
39. E.D. Potter, J.L. Herek, S. Pedersen, Q. Liu, A.H. Zewail: Nature **355**, 66 (1992)
40. T. Baumert, G. Gerber: Phys. Scr. T. **72**, 53 (1997)
41. T. Frohnmeyer, M. Hofmann, M. Strehle, T. Baumert: Chem. Phys. Lett. **312**, 447 (1999)
42. M. Machholm, A. Suzor-Weiner: J. Chem. Phys. **105**, 971 (1996)
43. J.A. Fleck, J.R. Morris, M.D. Feit: Appl. Phys. **10**, 129 (1976)
44. A. Giusti-Suzor, X. He, O. Atabek, F.H. Mies: Phys. Rev. Lett. **64**, 515 (1990)
45. C. Meier, V. Engel: Phys. Rev. Lett. **73**, 3207 (1994)
46. V. Engel: private communication (1999)
47. A. Assion, T. Baumert, J. Helbing, V. Seyfried, G. Gerber: Phys. Rev. A **55**, 1899 (1997)
48. B. Broers, H.B. van Linden van den Heuvell, L.D. Noordam: Phys. Rev. Lett. **69**, 2062 (1992)
49. J.S. Melinger, S.R. Gandhi, A. Hariharan, D. Goswami, W.S. Warren: J. Chem. Phys. **101**, 6439 (1994)
50. J.S. Melinger, A. Hariharan, S.R. Gandhi, W.S. Warren: J. Chem. Phys. **95**, 2210 (1991)
51. J. Cao, C.J. Bardeen, K.R. Wilson: Phys. Rev. Lett. **80**, 1406 (1998)
52. B. Kohler, V.V. Yakolev, J. Che, J.L. Krause, M. Messina, K.R. Wilson, N. Schwentner, R.M. Whitnell, Y. Yan: Phys. Rev. Lett. **74**, 3360 (1995)
53. J.M. Papanikolas, R.M. Williams, S.R. Leone: J. Chem. Phys. **107**, 4172 (1997)
54. C.J. Bardeen, Q. Wang, C.V. Shank: Phys. Rev. Lett. **75**, 3410 (1995)
55. D.W. Schumacher, J.H. Hoogenrad, Dan Pinkos, P.H. Bucksbaum: Phys. Rev. A **52**, 4719 (1995)
56. T.C. Weinacht, J. Ahn, P.H. Bucksbaum: Nature **397**, 233 (1999)
57. C.J. Bardeen, J. Che, K.R. Wilson, V.V. Yakolev, P. Cong, B. Kohler, J.L. Krause, M. Messina: J. Phys. Chem. A **101**, 3815 (1997)
58. V.V. Yakolev, C.J. Bardeen, J. Che, J. Cao, K.R. Wilson: J. Chem. Phys. **108**, 2309 (1998)
59. V.V. Lozovoy, S.A. Antipin, F.E. Gostev, A.A. Titov, D.G. Tovbin, O.M. Sarkisov, A.S. Vetchinkin, S.Y. Umanskii: Chem. Phys. Lett. **284**, 221 (1998)
60. A. Assion, T. Baumert, J. Helbing, V. Seyfried, G. Gerber: Chem. Phys. Lett. **259**, 488 (1996)
61. V. Engel: Comput. Phys. Commun. **63**, 228 (1991)
62. C. Meier, V. Engel: Femtosecond Chem., ed. by J. Manz, L. Wöste (VCH, Weinheim 1995) p. 369
63. S. De Silvestri, P. Laporta, O. Svelto: IEEE J. Quantum Electron. **QE-20**, 533 (1984)